AD-A091 120 NATIONAL AERONAUTICS AND SPACE ADMINISTRATION CLEVEL--ETC F/G 21/5
EXPERIMENTAL PERFORMANCE AND ANALYSIS OF 15.04-CENTIMETER-TIP-D--ETC(U)
OCT 80 K L MCLALLIN, J E HAAS

UNCLASSIFIED NASA-E-391 NASA-TP-1730 NL

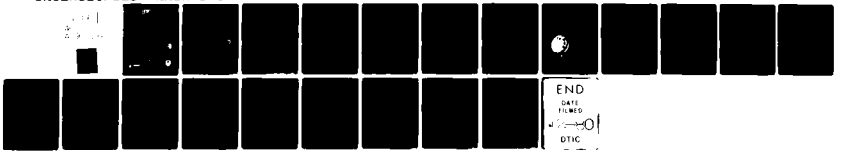

END
DATE FILMED
DTIC

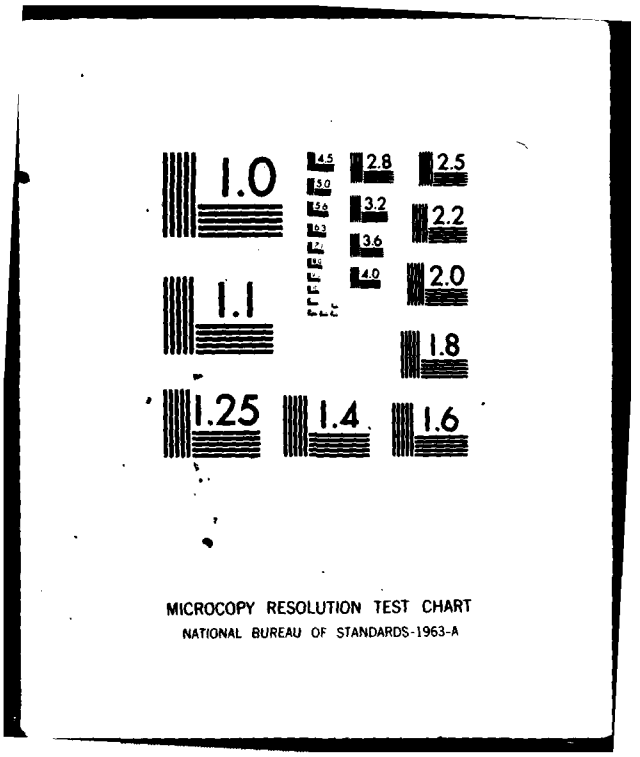
1.0
1.1
1.25
1.4
1.6
1.8
2.0
2.2
2.5
2.8
3.2
3.6
4.0
4.5
5.0
5.6
6.3
MICROCOPY RESOLUTION TEST CHART
NATIONAL BUREAU OF STANDARDS-1963-A

(1)

(9) NASA Technical Paper 1730

AVRADCOM Technical Report 80-09

(12) 22 (18) NASA, USAAVRADCOM

(19) TP-1730, TR-80-09

(6)

Experimental Performance and Analysis of 15.04-Centimeter-Tip-Diameter, Radial-Inflow Turbine With Work Factor of 1.126 and Thick Blading.

(11) Oct 80

(10) Kerry L. McLallin Jeffrey E. Haas
~~Lewis Research Center~~
Cleveland, Ohio

Jeffrey E. Haas
Propulsion Laboratory
AVRADCOM Research and Technology Laboratories
Lewis Research Center
Cleveland, Ohio

(14) NASA-E-392

National Aeronautics and Space Administration

Scientific and Technical Information Branch

1980

387544

Summary

The aerodynamic design, the experimental performance, and an internal loss breakdown are presented for a 15.04-centimeter-tip-diameter, radial-inflow turbine designed to drive a two-stage, 10-to-1 pressure ratio compressor that has a mass flow of 0.952 kilogram per second. For this application the rotative speed was 70 000 rpm and the turbine inlet temperature was 1478 K. The turbine was designed for this high-temperature application and has blades thick enough to accommodate internal cooling passages and trailing-edge coolant ejection. The turbine was fabricated and tested with solid, uncooled blading. The rotor tip diameter was limited to 86 percent of optimum in order to reduce tip speed. The resulting design-point work factor was 1.126.

The performance tests were conducted in air at nominal turbine inlet conditions of 1.379×10^5 N/m^2 and 322.2 K, which yield the design Reynolds number at corrected design values of mass flow and speed. Data were obtained at corrected speeds from 0 to 110 percent of design and at corrected ratios of turbine inlet total to rotor exit static pressure from 1.2 to 4.7. The experimental performance results show that for corrected design values of speed and total-to-static pressure ratio the corrected mass flow was 0.2372 kilogram per second (2.55 percent greater than design) and the corrected torque was 4.702 newton-meters (3.25 percent less than design). The turbine static efficiency for these conditions was 0.788, 4.6 points less than design; the corresponding total efficiency was 0.827, 5.3 points less than design. The peak total efficiency (0.842) occurred near the theoretically optimum values of work factor (0.83) and blade-jet speed ratio (0.70).

A breakdown of the internal losses was made to obtain an insight into the causes for the 5.3-point deficit in total efficiency between design and test. Three loss areas, not considered in the turbine design, were identified as responsible for the deficit in efficiency. These losses—stator secondary flows, vaneless-space surface friction, and trailing-edge wake mixing—resulted in penalties of 2.42, 1.05, and 1.80 efficiency points, respectively. This investigation showed that compromises in geometry can significantly affect turbine performance. The aerodynamic effects of these compromises must be investigated either analytically or experimentally for accurate prediction of design performance.

Introduction

The performance of small gas turbine engines (1.0 kg/sec and 225 to 375 kW) has not kept pace with the performance achieved in larger engines. Major factors in this performance difference are component efficiency and inlet temperature capability. Both factors are lower for small turbines. In an effort to improve small-turbine efficiency and high-inlet-temperature capability, a small-turbine technology program was undertaken at the Lewis Research Center. As part of this program, baseline levels of achievable performance and the aerodynamic penalties incurred from cooling are being evaluated for small axial- and radial-inflow turbines.

A compressor drive turbine application for a two-stage, 10-to-1 pressure ratio compressor with a mass flow rate of 0.952 kilogram per second was selected as representing an advanced turbine application in this size class. The turbines designed for this application have a turbine inlet temperature of 1478 K and a rotative speed of 70 000 rpm.

Two single-stage, axial-flow turbines were designed. Both have a tip diameter of 12.766 centimeters and a work factor of 1.7. Near symmetrical vector diagrams and optimum solidity were also selected. An uncooled version, with an aspect ratio of 1.0, was designed for baseline performance tests. The cooled version, with an aspect ratio of 0.5, was designed with blades thick enough to accommodate internal cooling passages and trailing-edge ejection of the coolant. The aerodynamic performance results for these two configurations are reported in references 1 and 2.

Radial-inflow turbines are of interest for small-engine applications because they have demonstrated higher levels of efficiency than small axial-flow turbines in uncooled applications. To achieve this performance advantage, radial-inflow turbines with radial inlet blading must operate at a tip speed high enough to give blade-jet-speed-ratio and work-factor values of about 0.70 and about 0.83, respectively. For advanced applications with high turbine inlet temperatures, operation at optimum values of blade-jet speed ratio and work factor is not always possible even with internal cooling. The selection of these values can be based on stress-life considerations or such other system requirements as inertia and off-design performance. When tip speed limits are severe, turbine aerodynamic performance may be heavily penalized.

The radial-turbine part of the small-turbine technology program has three objectives. The first is to evaluate the baseline performance of a design that has an arbitrary limit on tip speed. The second is to apply a well-developed cooling scheme to this design. The third is to evaluate the aerodynamic penalties (if any) associated with the selected cooling scheme.

The single-stage, radial turbine for the previously described application has an arbitrarily selected tip diameter of 15.04 centimeters. The resulting blade-jet speed ratio and work factor are 0.609 and 1.126, respectively. During the preliminary design phase the turbine was designed with blades thick enough to accommodate internal cooling and trailing-edge coolant ejection. The final cooling scheme was selected from a competitive procurement involving leading manufacturers of small gas turbine engines and leading research organizations in the United States. The primary selection criterion was that the cooling scheme be based on reasonably well-developed cooling technology. The selected cooling scheme, conduction cooling of the turbine rotor, was achieved by fabricating the second-stage compressor impeller back to back with the turbine rotor. (The result was designated a "monorotor.") Leakage from the compressor impeller to the turbine rotor was assumed to film cool the rotor hub. During the design phase for the monorotor it was found that hub profile differences between the compressor and the turbine caused larger than desired centrifugal stresses. In the final design the turbine meridional flowpath was changed to reduce both the centrifugal stress and the exducer temperature. The final design also had thick blading to facilitate conduction cooling. The design and mechanical testing of the monorotor are presented in reference 3.

The fabrication of the solid-bladed test version of the original radial turbine was nearly complete when it was found to be incompatible with the monorotor concept. However, the aerodynamic testing of this original design was completed because it still should give a valid baseline for designs that operate at tip speeds that are about 86 percent of the optimum value and that have thick blading for accommodating either internal cooling and trailing-edge ejection or conduction cooling (as in a monorotor). Since the blading was solid for this test, additional trailing-edge-wake mixing losses were incurred.

This report presents the aerodynamic design of the original 15.04-centimeter-tip-diameter radial turbine, the results of the aerodynamic tests, and a breakdown of the aerodynamic losses. The tests were conducted in air at nominal turbine inlet conditions of 1.379×10^5 N/m^2 and 322.2 K. At these conditions the hot-engine Reynolds number was obtained at corrected design values of mass flow and speed. Data were obtained at speeds from 0 to 110 percent of corrected design speed at corrected ratios of turbine inlet total to rotor exit static pressure from 1.2 to 4.7. The overall performance is presented in terms of mass flow, torque, specific work, and efficiency. Rotor inlet and rotor exit surveys were taken at design point, and the results are presented along with the calculated experimental velocity diagrams. The results of a study, based on analytical methods and experimental data, to assess turbine internal losses are also presented.

Symbols

A	flow area, cm^2
c	chord, cm
d	flow deviation angle, $\beta - \psi$, deg
h	passage height, cm
Δh	specific work, J/kg
N_s	specific speed, $NQ^{1/2}/(\Delta h_{id}')^{3/4}$
N	turbine wheel speed, rad/sec
n	blade normal thicknesses, cm
P	absolute pressure, N/m^2
p	vane surface coordinate, cm
Q	volume flow rate, m^3/sec
R	gas constant, J/kg K
Re	turbine Reynolds number, $w/\mu r_T$
r	radius from turbine centerline, cm
s	blade spacing, cm
T	absolute temperature, K
U	blade speed, m/sec
V	absolute flow velocity, m/sec
W	relative flow velocity, m/sec
w	mass flow rate, kg/sec
x	axial coordinate along rotation axis
y	horizontal coordinate perpendicular to rotation axis
z	vertical coordinate perpendicular to rotation axis
α	absolute flow angle, deg
β	relative flow angle, deg
Γ	torque, N-m
γ	ratio of specific heats
δ	ratio of turbine inlet total pressure to U.S. standard sea-level pressure, P_1'/P^*

ϵ specific-heat-ratio correction,

$$\frac{\gamma^*[2/(\gamma^*+1)]^{\gamma^*/(\gamma^*-1)}}{\gamma[2/(\gamma+1)]^{\gamma/(\gamma-1)}}$$

η efficiency

θ squared ratio of inlet critical velocity to U.S. standard sea-level critical velocity, $(V_{cr}/V^*_{cr})^2$

λ work factor, $\Delta h'/U_T^2$

μ viscosity, N sec/m^2

ν blade-jet speed ratio, $U_T/(2\,\Delta h_{id})^{1/2}$

φ angle about rotation axis, deg

ψ blade metal angle, deg

Subscripts

cr conditions at Mach 1

id ideal flow process

l lower surface

m mean

T rotor inlet tip

t tip

u upper surface

v vane coordinate

x axial component

1 station at inlet to stator inlet plenum, or turbine inlet

2 station at stator trailing edge

3 station at rotor inlet (stator exit survey radius)

4 station at rotor exit (rotor exit survey plane)

5 station in exit duct

Superscripts

$(\bar{\ })$ average value

$()'$ total-state condition

$(^*)$ U.S. standard sea-level condition

Turbine Design

The subject radial-inflow turbine was designed to drive a two-stage, 10-to-1 pressure ratio compressor with a mass flow of 0.952 kilogram per second and a rotative speed of 70 000 rpm. The design-point turbine inlet temperature is 1478 K. Turbine design operating conditions are given in table I. The rotor tip diameter of 15.04 centimeters was chosen to give a reduced-tip-speed design. The resulting rotor tip speed is about 86 percent of the optimum value for a radial-bladed inducer at the required work level.

TABLE I.—TURBINE DESIGN CONDITIONS

	Hot	Corrected[a]
Inlet total temperature, T_1', K	1478	288.2
Inlet total pressure, P_1', N/m^2	9.101×10^5	1.013×10^5
Rotative speed, N, rpm	70 000	31 456
Mass flow rate, w, kg/sec	0.8918	0.2313
Specific work, Δh, J/g	342.7	69.2
Total-to-total pressure ratio, P_1'/P_4'	2.793	3.028
Total-to-static pressure ratio, P_1'/P_4	2.977	3.255
Total efficiency, $\eta_{1\text{-}4}'$	0.880	0.880
Static efficiency, $\eta_{1\text{-}4}$	0.834	0.834
Work factor, λ	1.126	1.126
Specific speed, N_s	0.470	0.464
Blade-jet speed ratio, ν	0.609	0.609
Reynolds number, Re	2.28×10^5	1.71×10^5

[a]U.S. standard sea-level conditions.

Efficiency Evaluation

The design total efficiency level was based on a review of available radial-turbine data, including the specific-speed study of reference 4. From this performance data it was determined that, because of the reduced-tip-speed design, the total efficiency should be reduced by 2 points to the design value of 0.88. Since the turbine would eject coolant from the thick trailing edges, additional mixing losses due to the trailing-edge blockage effects were not included; however, the design efficiency does include the mixing losses associated with an uncooled, "thin" blading design.

Velocity Diagram

The design-point vector diagrams were calculated for a total efficiency of 0.88. Based on the assumption of 2 percent total-pressure loss in the stator, the loss split was 1.8 and 10.2 efficiency points for the stator and the rotor, respectively.

The design velocity diagram is shown in figure 1. The stator has radial flow at the inlet and 76° of turning. The exit absolute flow angle is near optimum for this radial turbine, which has a specific speed of 0.470 (ref. 5). Although all free-stream velocities are subsonic, the absolute velocity within the vaneless space is high, with a rotor inlet absolute critical velocity ratio of 0.897. The rotor incidence is 16.5°; the optimum incidence for a 12-blade rotor is -36.7° (ref. 5). The rotor also has negative swirl at the exit, which is a positive contribution to turbine work output.

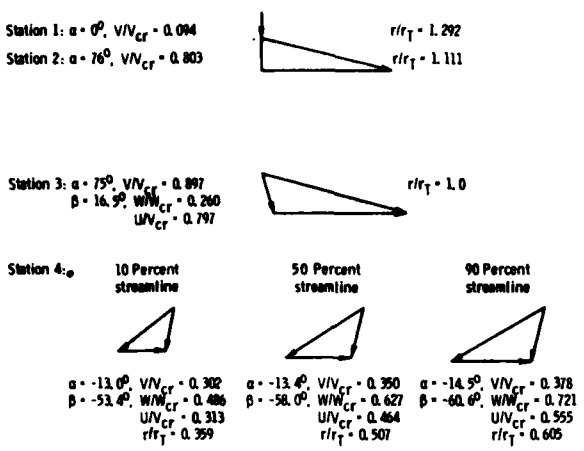

Figure 1. - Design-point velocity diagrams.

Stator

The stator has 29 vanes with a radial-flow inlet from a low-Mach-number plenum. The design exit angle is 76°. The stator solidity and aspect ratio are 1.69 and 0.265, respectively, based on the stator exit radius and the actual chord. The trailing-edge thickness of 0.0813 centimeter amounts to 18.6 percent blockage and results from the physical requirements of ejecting coolant from the trailing edge. Stator geometric parameters are presented in table II. Figure 2 shows a sector of the turbine flowpath in which the stator vane configuration can be seen.

The stator vane surface profile was designed to give an acceptable loading diagram having a smooth velocity profile along the surface with only minor regions of diffusion. The design loading diagram along the 50 percent streamline is presented in figure 3. Both blocked and unblocked free-stream velocities are shown at the vane leading and trailing edges. After the flow is past the leading-edge region, at 25 percent of the meridional distance, both suction- and pressure-surface velocities increase to the vane exit. This type of loading diagram should yield low profile losses. This design loading diagram was calculated by using the MERIDL and TSONIC computer programs (refs. 6 and 7, respectively).

Vaneless Space

The vaneless space between the stator exit and the rotor inlet is relatively long, with a stator-exit-to-rotor-inlet diameter ratio of 1.111. This long vaneless space length (1.5 times the stator chord length) results from the combination of two design criteria: (1) selecting a near-optimum stator exit angle based on the turbine specific-speed correlation, and (2) selecting a reduced-tip-diameter rotor design for a high-work-factor application. The experimental results of reference 8, however, indicate that minimum vaneless-space losses occur between diameter ratios of 1.06 and 1.11. The design diameter ratio is close to this optimum range, and no additional loss was assumed.

Rotor

The rotor has 12 full blades thick enough to allow internal cooling passages and the trailing-edge ejection of coolant. An axial view of the rotor flowpath is shown in figure 2, and the actual rotor is shown in figure 4. The figures show that the rotor has radial blades at the inducer inlet. The large flow blockages resulting from the thick trailing edges are 78.7, 38.2, and 14.9 percent at the hub, mean, and tip, respectively. In the turbine tests presented herein the blading is solid with no coolant ejection. The mixing losses resulting from the high blading flow blockage in both the stator and the rotor will result in some decrease in turbine efficiency from the design value. The rotor tip-to-shroud clearances are typical for this size of radial turbine with inlet (axial) and exit (radial) clearances of 3.7 and 1.2 percent of passage height, respectively. Rotor geometric parameters are given in table II.

TABLE II.—TURBINE BLADING GEOMETRY

Rotor inlet diameter, cm	15.04
Ratio of rotor exit tip to inlet diameters	0.6275
Ratio of rotor exit hub to tip diameters	0.4844
Ratio of stator exit to rotor inlet diameters	1.111
Ratio of stator inlet vane height to rotor inlet diameter	0.0726
Ratio of stator exit vane height to rotor inlet diameter	0.0537
Ratio of stator inlet to stator exit diameters	1.163
Number of stator vanes	29
Number of rotor blades	12
Stator leading-edge thickness, cm	
(percent of $s \cos \alpha$)	0.3556 (16.9)
Stator trailing-edge thickness, cm	
(percent of $s \cos \alpha$)	0.0813 (18.6)
Rotor leading-edge thickness, cm (percent of $s \cos \beta$):	
Hub	0.5994 (15.9)
Mean	0.4661 (12.4)
Shroud	0.2388 (6.3)
Rotor trailing-edge thickness, cm (percent of $s \cos \beta$):	
Hub	0.6894 (78.7)
Mean	0.3835 (38.2)
Shroud	0.1778 (14.9)
Rotor-shroud clearance, cm (percent of h):	
Inlet (axial)	0.030 (3.7)
Exit (radial)	0.030 (1.2)

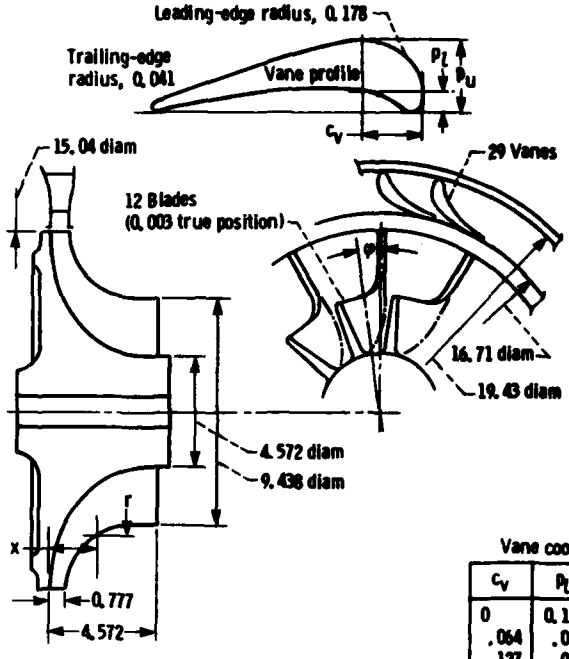

Rotor blade camber line

Tip				Hub			
x	r	φ	n	x	r	φ	n
0.777	7.521	0°	0.239	0	7.521	0°	0.599
.777	7.338		.244	.003	7.259		.574
.785	7.112		.254	.020	6.736		.676
.808	6.858		.279	.071	6.218		.754
.853	6.604		.297	.170	5.697		.810
.927	6.33		.31	.333	5.199		.846
1.052	6.02		.315	.546	4.719		.859
1.232	5.72		.312	.803	4.262		.853
1.463	5.443		.302	1.105	3.835		.831
1.742	5.212		.284	1.461	3.447		.795
2.057	5.029	0° 10'	.264	1.862	3.106		.752
2.395	4.892	0° 38'	.241	2.301	2.824	0° 5'	.709
2.758	4.796	1° 37'	.216	2.776	2.598	1° 27'	.676
3.099	4.745	3° 24'	.216	3.274	2.433	4° 27'	.658
3.467	4.724	6° 23'	.234	3.782	2.332	9° 39'	.668
3.853	4.719	10° 34'	.259	4.046	2.301	14° 23'	.782
4.211	4.719	15° 48'	.29	4.572	2.286	21° 53'	.589
4.572	4.719	21° 53'	.178	-----	-----	------	

Vane coordinates

c_v	p_l	p_u
0	0.178	0.178
.064	.041	.320
.127	.008	.394
.191	0	.455
.254	.018	.503
.318	.041	.541
.381	.064	.566
.508	.102	.582
.635	.13	.577
.762	.147	.559
.889	.157	.531
1.016	.160	.500
1.143	.157	.465
1.270	.15	.429
1.397	.14	.391
1.524	.127	.353
1.651	.114	.315
1.778	.097	.277
1.905	.079	.239
2.032	.061	.203
2.159	.043	.173
2.286	.025	.132
2.413	.008	.102
2.477	0	.084
2.522	.041	.041

Figure 2. - Blading geometry for 15.04-centimeter-diameter radial-inflow turbine. (Dimensions are in centimeters.)

The rotor blade profile was developed by using the MERIDL and TSONIC programs. The profile was developed to have smooth surface velocity distributions and to minimize flow diffusion within the constraints of radial inlet blading and no splitter blades. Figure 5 shows the rotor loading diagrams along the 10, 50, and 90 percent streamlines. The blocked and free-stream rotor inlet and exit velocity levels are shown in the figure and demonstrate the large effect that the thick trailing edges have on velocity at the exit. The blades are highly loaded at the inlet, and the hub and mean streamline loading diagrams indicate large diffusions on the suction surface near 60 percent of the meridional distance. However, the rapid flow acceleration from this point to the rotor exit should minimize the surface friction

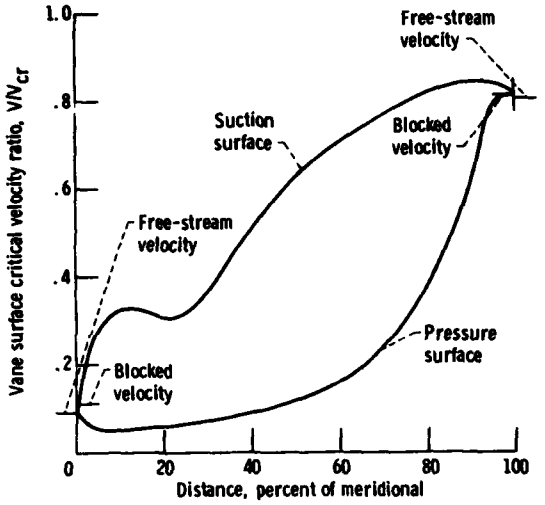

Figure 3. - Stator vane design-point loading diagram for 50 percent streamline.

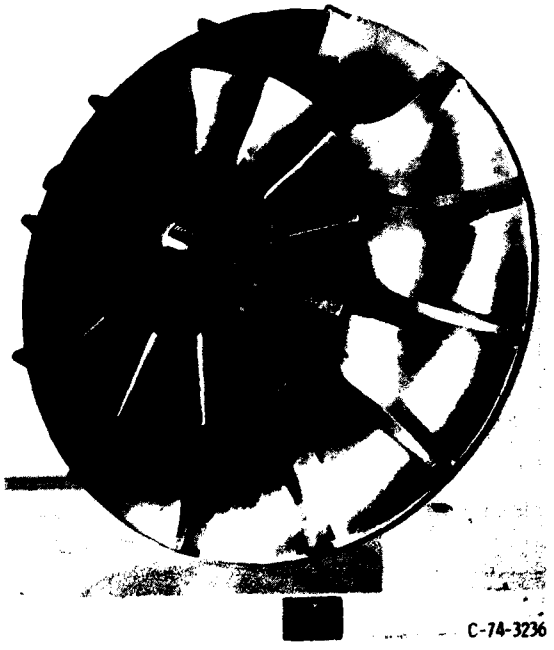

Figure 4. - Turbine rotor.

losses that occur because of this diffusion. The results of reference 9 indicate that no penalty in efficiency will result from using a rotor without splitter blades, as the increased losses due to high inlet loading are offset by the elimination of the surface friction and mixing losses from the splitter blades.

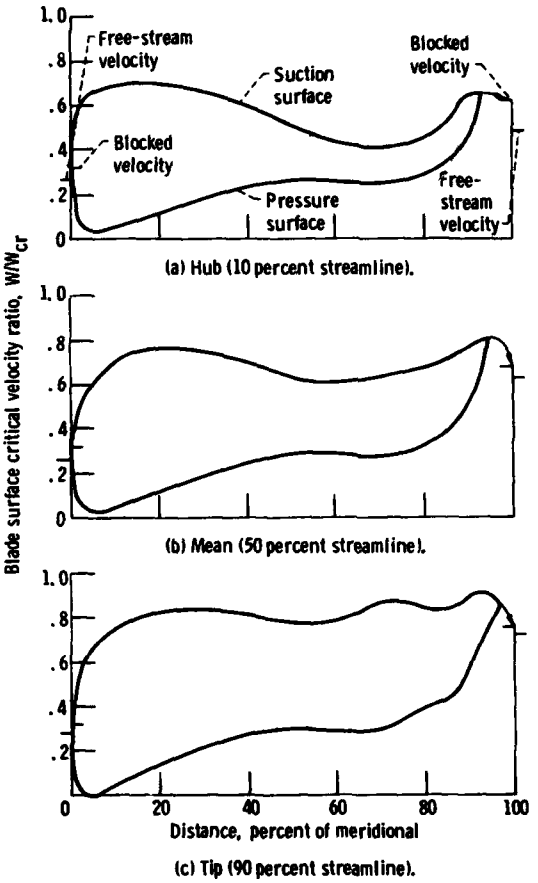

(a) Hub (10 percent streamline).

(b) Mean (50 percent streamline).

(c) Tip (90 percent streamline).

Figure 5. - Rotor design-point loading diagrams.

Apparatus, Instrumentation, and Procedure

The apparatus used in this investigation consisted of the turbine test package, an airbrake dynamometer to absorb and measure turbine torque, an inlet and exhaust piping system including flow controls, and the research instrumentation. A schematic of the experimental equipment is shown in figure 6, and a cross section of the turbine test package is shown in figure 7.

At the scroll inlet, station 1, both static pressure and total temperature were measured, as shown in figure 8(a). Four static-pressure taps were equally spaced about the circumference of the inlet pipe. Three total-temperature rakes, each with two thermocouples, were located as shown in the figure.

At the stator exit, station 2, wall static pressures were measured midway between the suction and pressure surfaces just upstream of the trailing edge.

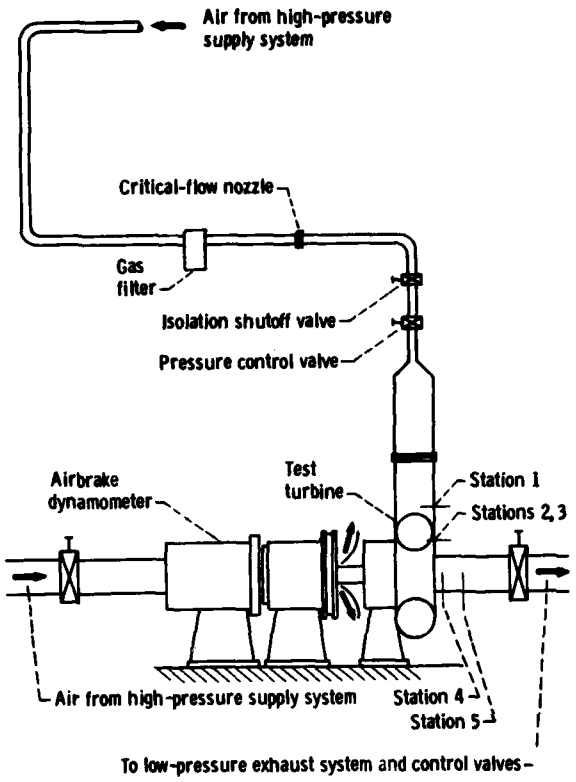

Figure 6. - Experimental equipment.

There were eight taps, four each on the disk-side and shroud-side walls, equally spaced around the circumference, as shown in figure 8(b) for the shroud-side wall.

At the rotor inlet, station 3, static pressure was measured just upstream of the rotor leading edge with six taps, three each on the disk-side and shroud-side walls, equally spaced circumferentially, as shown in figure 8(b). Total pressure and flow angle were measured axially and circumferentially over about two vane passages. Two probes were used separately: First, a self-balancing probe was used to measure flow angle; and second, a single-element total-pressure probe set at the local free-stream value of measured flow angle was used to measure total pressure.

At the rotor exit, station 4, about 2.8 centimeters (115 percent of the exit blade height) downstream of the rotor trailing edge, static pressure, total pressure, total temperature, and flow angle were measured as shown in figure 8(c). Eight static-pressure taps, four each on the hub and shroud walls, were equally spaced about the circumference. The four hub taps were interconnected to give an average static-pressure reading. A combination probe was used to survey the total pressure, total temperature, and flow angle from the hub to the shroud at the rotor exit at one circumferential position. The probe-actuator system used is described in reference 10. Turbine exit total temperature was also measured downstream of the rotor exit survey plane in the exit duct, as shown in figure 8(c) at station 5. This plane is about 13.7 centimeters downstream of the rotor trailing edge. The three two-element thermocouple probes were equally spaced circumferentially.

The rotational speed of the turbine was measured with an electric counter in conjunction with a magnetic pickup and a shaft-mounted gear. Mass flow was measured with a calibrated critical-flow nozzle. An airbrake dynamometer was used to absorb the torque output of the turbine. The airbrake was supported on trunnion gas bearings, and the dynamometer torque was measured with a commercial strain-gage load cell.

The friction torque from the bearings, the seal, and the coupling windage was obtained by driving the rotor and shaft over the range of speeds covered in this investigation. The turbine cavity was evacuated to a pressure of about 150.0 N/m^2 for

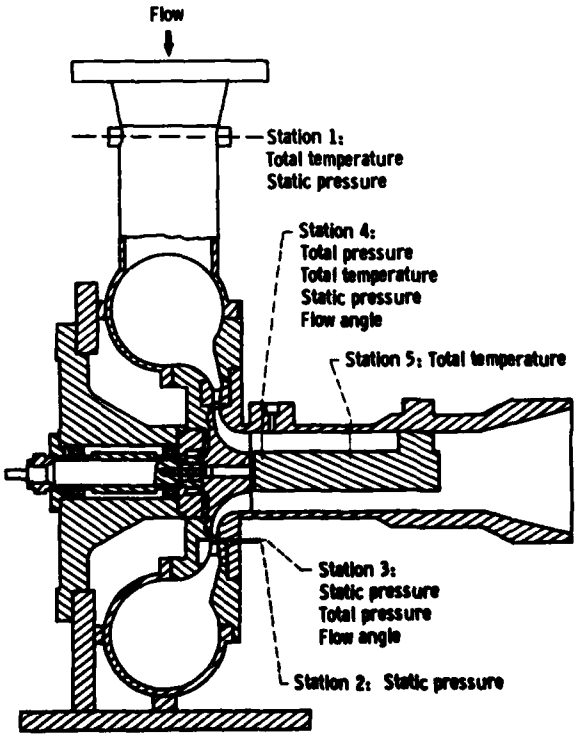

Figure 7. - Cross section of turbine test package.

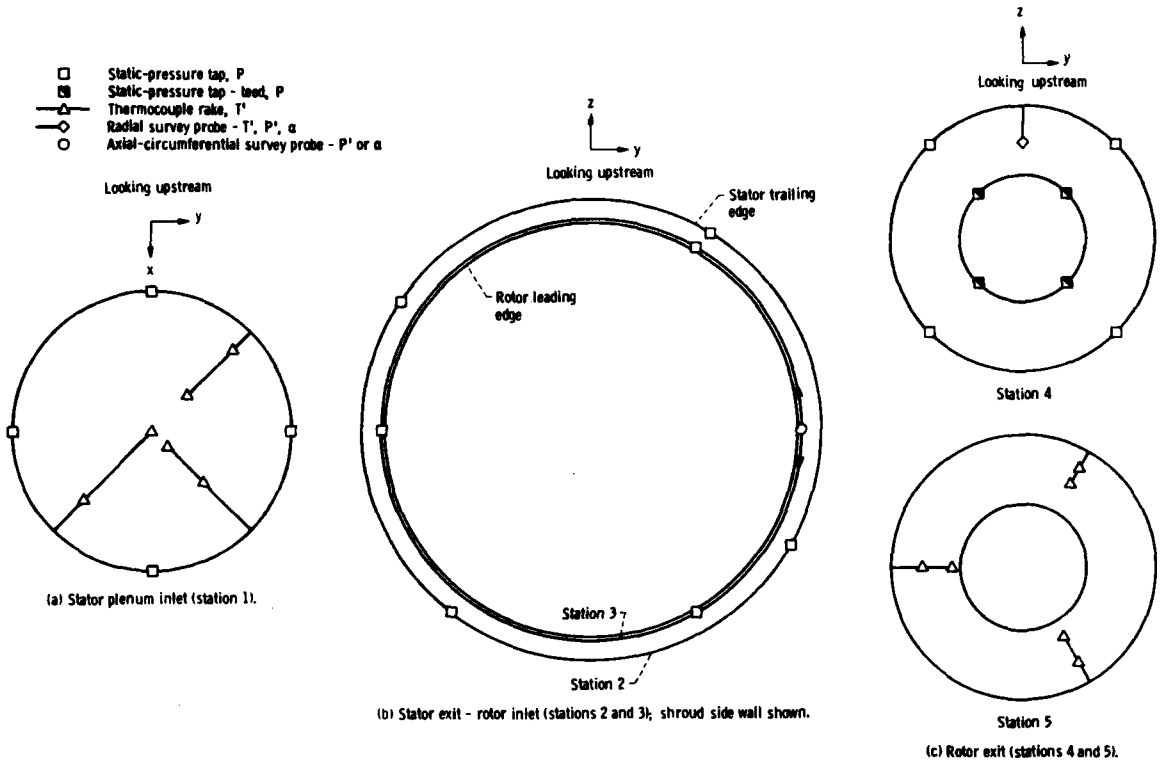

(a) Stator plenum inlet (station 1).

(b) Stator exit - rotor inlet (stations 2 and 3); shroud side wall shown.

(c) Rotor exit (stations 4 and 5).

Figure 8. - Turbine research instrumentation.

these tests in order to eliminate disk windage and blade pumping losses from the friction torque. At corrected design-point operation for the test conditions used, the friction torque was 0.18 newton-meter. This value of friction torque is 2.9 percent of the dynamometer torque at the corrected design point. Friction torque was added to dynamometer torque to obtain the turbine aerodynamic torque.

Data were obtained at nominal inlet total-state conditions of 322.2 K and 1.379×10^5 N/m^2. At these conditions the design hot Reynolds number is obtained when operating at the corrected design values of mass flow and speed. The turbine was operated over a range of corrected speeds from 0 to 110 percent of design and over a range of turbine-inlet-total- to rotor-exit-static-pressure ratios $P_1'/\bar{P}_4$ from 1.2 to 4.7.

The turbine was rated on the basis of both total and static efficiency. The total pressures used to obtain these efficiencies were calculated from mass flow w, static pressure P, total temperature T', and flow angle α with the following equation:

$$P' = P\left\{\frac{1}{2} + \frac{1}{2}\left[1 + \frac{2R(\gamma-1)}{\gamma}\left(\frac{w(T')^{1/2}}{\bar{P}A\cos\alpha}\right)^2\right]^{1/2}\right\}^{\gamma/(\gamma-1)}$$

In calculating turbine inlet total pressure P_1', the flow angle α_1 was assumed to be zero. In calculating rotor exit total pressure P_4', the total temperature T_4' is an average value based on measured torque, and the rotor exit flow angle α_4 is measured at the mean radius.

Results and Discussion

The experimental performance of a 15.04-centimeter-tip-diameter, radial-inflow turbine with thick vanes and blades has been determined in air at nominal turbine inlet conditions of 1.379×10^5 N/m^2 and 322.2 K. These conditions yield the design

Reynolds number for operation at corrected design values of mass flow and speed. Data were obtained at corrected speeds from 0 to 110 percent of design and at turbine-inlet-total- to rotor-exit-static-pressure ratios $P_1'/\bar{P}_4$ from 1.2 to 4.7. The overall performance is presented in terms of mass flow, torque, specific work, and efficiency. Rotor inlet and rotor exit surveys were taken at test conditions corresponding to corrected design values of speed and pressure ratio. The results are presented, along with the calculated experimental velocity diagram. The results of an analytical study to assess turbine internal losses are also presented.

Overall Performance

Mass Flow

The variation in turbine corrected mass flow is presented in figure 9 for lines of constant corrected speed over the range of turbine-inlet-total- to rotor-exit static-pressure ratios $P_1'/\bar{P}_4$ tested. At design corrected speed and the design corrected static pressure ratio $P_1'/\bar{P}_4$ of 3.255, the mass flow was 0.2372 kilogram per second, about 2.55 percent greater than design. Turbine mass flow increased with increasing static-pressure ratio and with decreasing speed. The high-speed lines stay separated at the high pressure ratios, indicating that the flow was controlled by the rotor. However, the low-speed lines tend to converge at high pressure ratios, and the zero speed line crosses over the 30, 50, 70, and 90 percent speed lines. This phenomenon is probably due to the high rotor incidence losses and the resulting reduction in rotor effective throat area in the low-speed, high-pressure-ratio regime.

Torque

Turbine corrected torque is presented in figure 10 for lines of constant corrected speed over the range of total-to-static pressure ratio $P_1'/\bar{P}_4$ tested. At design speed and the design $P_1'/\bar{P}_4$ of 3.255, turbine torque was 4.702 newton-meters, about 3.25 percent less than design. Turbine torque increased with decreasing speed and increasing pressure ratio. Since torque increased over the entire range of speeds and pressure ratios tested, limiting loading was not reached.

At the design $P_1'/\bar{P}_4$ of 3.255 a corrected torque of 4.702 newton-meters (3.25 percent less than design) combined with a corrected mass flow of 0.2372 (2.55 percent greater than design) indicates that the turbine static efficiency will be 5.6 percent (4.6 efficiency points) less than the design value of 0.834.

Turbine Exit Flow Angle

The rotor exit absolute flow angle is presented in figure 11 for lines of constant corrected speed over the range of $P_1'/\bar{P}_4$ tested. The flow angle was measured with a single radial-survey probe located at the midspan position. The flow angles presented in figure 11 were used in calculating the rotor exit absolute total pressure, as described in the section Apparatus, Instrumentation, and Procedure. The

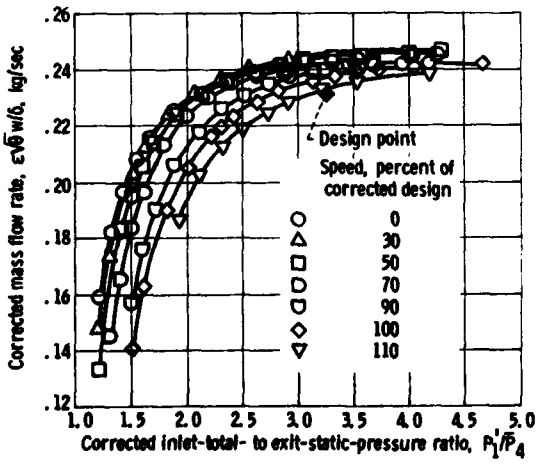

Figure 9. - Variation of mass flow rate with total-to-static pressure ratio for lines of constant speed.

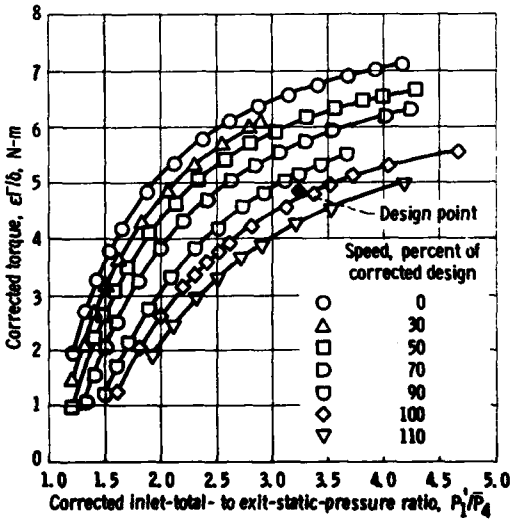

Figure 10. - Variation of torque with total-to-static pressure ratio for lines of constant speed.

figure shows that flow angle increased in the positive direction with increasing speed and decreasing pressure ratio. Flow angle is positive when the tangential momentum is in the direction of rotation; and at the rotor exit, negative flow angles indicate a positive contribution to turbine work output.

Total-Pressure Ratio

Turbine-inlet-total- to rotor-exit-total-pressure ratio P_1'/P_4' is presented in figure 12 for lines of constant corrected speed over the range of $P_1'/\bar{P}_4$ tested. At the design corrected total-to-static pressure ratio $P_1'/\bar{P}_4$ of 3.255, the total-to-total pressure ratio P_1'/P_4' increased with increasing speed and had a value of 3.045 at design corrected speed. This value of P_1'/P_4' is close to the design corrected value of 3.028.

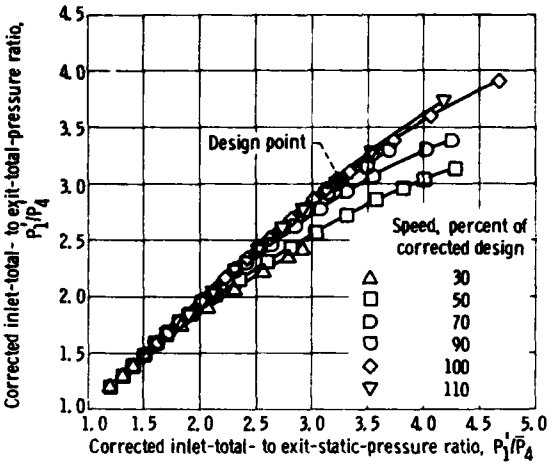

Figure 12. - Variation of total-to-total pressure ratio with total-to-static pressure ratio for lines of constant speed.

Turbine Efficiency

The turbine total and static efficiencies presented are calculated based on turbine inlet total pressure P_1' and on rotor exit total P_4' and static $\bar{P}_4$ pressures. Total and static efficiencies are presented in figures 13(a) and (b), respectively, as a function of blade-jet speed ratio for each speed tested. The optimum blade-jet speed ratio is about 0.7 for radial turbines with radial inlet blading, and the data presented in figure 13 are in agreement. The total efficiency (fig. 13(a)) decreased from its maximum of 0.842 as the blade-jet speed ratio changed from 0.7. The static efficiency (fig. 13(b)) similarly decreased from its maximum of 0.812 as blade-jet speed ratio changed from 0.7. The total and static efficiencies at the design blade-jet speed ratio of 0.609 were 0.827 and 0.788, respectively. Total efficiency is 5.3 points less than design, and static efficiency is 4.6 points less than design.

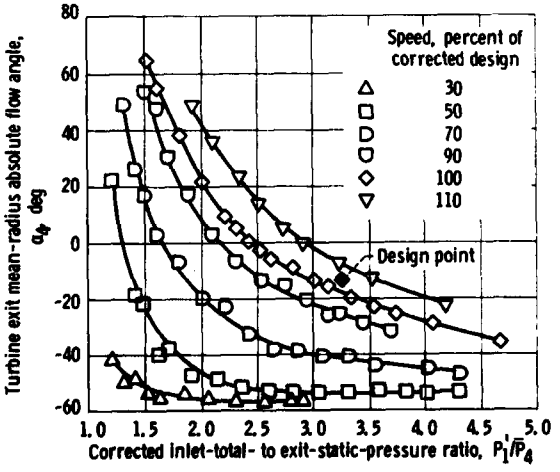

Figure 11. - Variation of turbine exit absolute flow angle with total-to-static pressure ratio for lines of constant speed.

Turbine Performance Maps

The overall turbine performance characteristics are presented in figure 14 in the form of performance maps. Specific work is plotted against the mass flow-speed parameter for lines of constant speed, with lines of constant turbine pressure ratio and constant efficiency superimposed. All quantities are corrected to U.S. standard sea-level conditions. Two performance points, corresponding to design work and to design total-to-static pressure ratio $P_1'/\bar{P}_4$ are presented in table III and shown on the 100 percent speed line in figure 14.

The performance map based on rotor exit total pressure is shown in figure 14(a). The efficiency at both design work and design total-to-total pressure ratio P_1'/P_4' was well below the maximum total efficiency contour of 0.84, thus showing the effects of nonoptimum aerodynamic design (a high-work-factor design point). At the design work factor of 1.126 and design speed the total efficiency was 0.824 and the P_1'/P_4' required was 3.31 (table III).

The performance map based on rotor exit static pressure is shown in figure 14(b). The efficiency at design work requirements was well below the maximum static efficiency contour of 0.81. At design work factor and design speed the static efficiency was 0.776 and the $P_1'/\bar{P}_4$ required was 3.62 (table III).

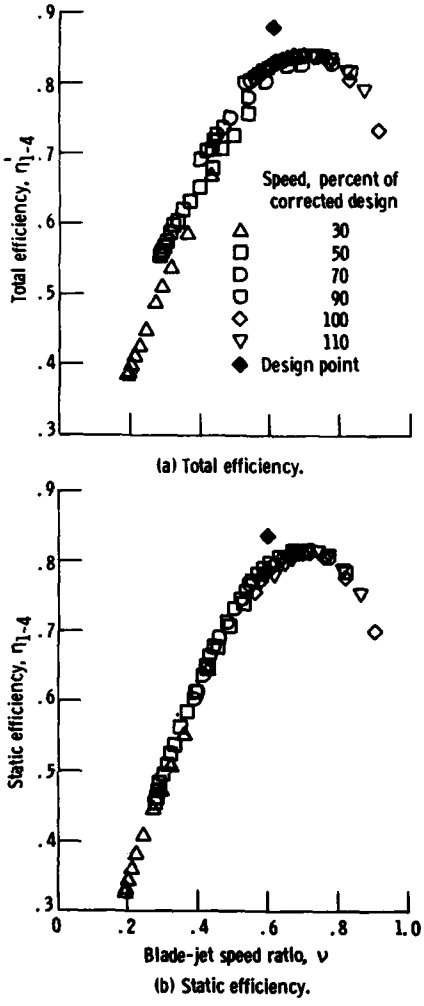

Figure 13. - Variation of efficiency with blade-jet speed ratio for lines of constant speed.

To illustrate the overall effect on performance of designing for high work factor, two constant-work-factor lines corresponding to the design work factor of 1.126 and to the theoretically optimum work factor of 0.833 (based on rotor incidence considerations, ref. 5) were superimposed on the performance maps (fig. 14). Operating the turbine along the high-work-factor line resulted in efficiencies well below the maximum level possible over the entire speed range. However, operating along the theoretical optimum-work-factor line resulted in turbine efficiencies at or near the maximum level possible over the entire speed range. This was true for both total and static efficiency. The total efficiency at the optimum work factor and at design speed was about 0.84 (fig. 14(a)), and rotor inlet flow conditions were optimum for this case. It was determined during the design phase for this turbine that a turbine total efficiency of 0.90 was possible at the optimum work factor. The lower level of peak efficiency attained by the subject turbine indicates that losses, other than those associated with rotor incidence, were greater than design intent. Two possible high-loss mechanisms applicable to this turbine are the surface friction losses generated by a long vaneless space and the wake mixing losses generated by the thick blading trailing edges.

Internal Flow Characteristics

Turbine Reaction

Turbine reaction is presented in figure 15 at design corrected speed in terms of the average-static- to inlet-total-pressure ratio $\bar{P}/P_1'$ for selected total-to-static pressure ratios $P_1'/\bar{P}_4$. The local static-to-total pressure ratio $\bar{P}/P_1'$ is shown in the figure at the plenum inlet, the stator exit, the rotor inlet, and the rotor exit.

Static pressure decreased (positive reaction) through both the stator and the rotor at all turbine pressure ratios tested. The pressure decrease through the vaneless space between stations 2 and 3 is also shown in figure 15. A 10 percent reduction in annulus flow area occurred from the stator exit to the rotor inlet. This reduction, combined with conservation of tangential momentum, will result in a flow velocity increase through the vaneless space if the total-pressure loss is relatively small.

The design static-pressure variation through the turbine is shown in figure 15 by the dashed line. Comparing the data with the design variation indicates that the stator is overexpanded at the design total-to-static pressure ratio $P_1'/\bar{P}_4$ of 3.255. This phenomenon is consistent with a mass flow measurement that was 2.55 percent higher than design (see section Mass Flow).

Rotor Inlet Survey

Surveys of absolute flow angle and absolute total pressure at the rotor inlet, station 3, were obtained at a stator-exit-static- to turbine-inlet-total-pressure ratio $\bar{P}_3/P_1'$ of 0.595. The surveys were made over two stator vane passages and at 11 axial positions from hub to shroud. Data were taken at 11 circumferential positions and arithmetically averaged. The results are presented in figure 16 as a function of the vaneless-space passage height. The

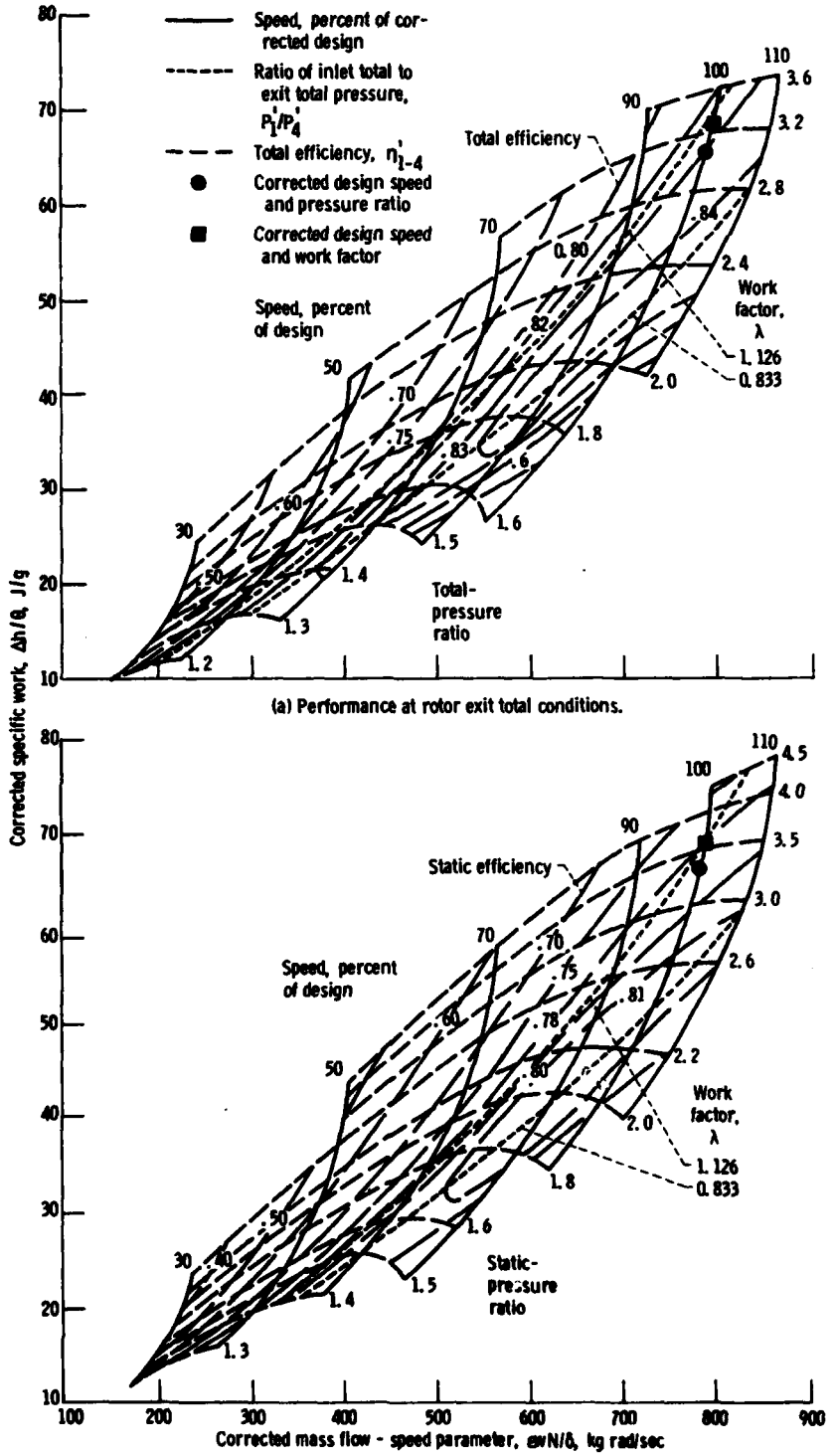

(a) Performance at rotor exit total conditions.

(b) Performance at rotor exit static conditions.

Figure 14. - Turbine performance maps based on conditions at turbine inlet and rotor exit.

TABLE III.—COMPARISON OF DESIGN AND EXPERIMENTAL PERFORMANCE

	Design	Experiment	
		Design work factor	Design pressure ratio
Inlet total temperature, T_1', K	1478	322.2	322.2
Inlet total pressure, P_1', N/m^2	9.101×10^5	1.379×10^5	1.379×10^5
Reynolds number, R_t	2.28×10^5	2.13×10^5	2.07×10^5
Corrected mass flow rate, $\epsilon\sqrt{\theta}w/\delta$, kg/sec	0.2313	0.2398	0.2372
Corrected specific work, $\Delta h/\theta$, J/g	69.2	69.2	65.3
Speed, percent of corrected design, $N/314.56\sqrt{\theta}$	100	100	100
Corrected total-to-total pressure ratio, P_4'/P_4'	3.028	3.310	3.045
Corrected total-to-static pressure ratio, P_1'/P_4	3.255	3.620	3.255
Total efficiency, η_{1-4}'	0.880	0.824	0.827
Static efficiency, η_{1-4}	0.834	0.776	0.788
Work factor, $\Delta h/U_T^2$	1.126	1.126	1.063

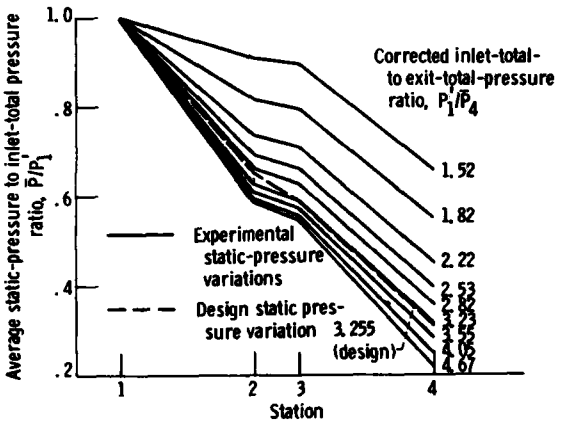

Figure 15. - Variation of static pressure through turbine at design speed.

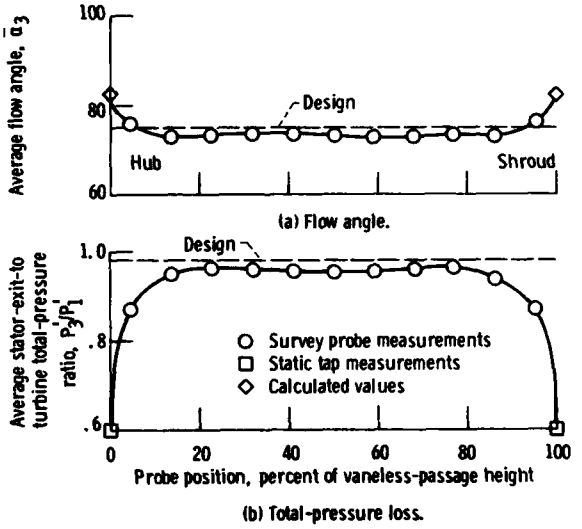

Figure 16. - Rotor inlet survey results at a stator static-to-total pressure ratio $\bar{P}_3/P_1'$ of 0.595.

flow angle shown in figure 16(a) was relatively constant over most of the passage and was from 1° to 2° less than the design value of 75.0°. The total-to-total pressure ratio $\bar{P}_3'/P_1'$ shown in figure 16(b) was relatively constant over the middle 80 percent of the passage height. Large total-pressure losses occurred near both endwalls.

The flow angles at the hub and shroud walls shown in figure 16(a) are those required to match continuity during computation of the mass-averaged flow conditions. The total pressures shown in figure 16(b) at the hub and shroud walls are the measured wall static pressures. The overall mass-averaged values of total pressure ratio $\bar{P}_3'/P_1'$ and flow angle α_3 were 0.937 and 73.6°, respectively; design values at the survey radius were 0.98 and 75.0°, respectively. The measured stator and vaneless-space total-pressure loss was 3.15 times the design value.

Rotor Exit Survey

A rotor exit radial survey was taken at one circumferential position for design corrected values of speed and rotor-exit-total- to turbine-inlet-total-pressure ratio P_4'/P_1'. The data, taken at 11 radial positions, are plotted in figure 17 against the rotor exit radius ratio. The variation in local P_4'/P_1' is

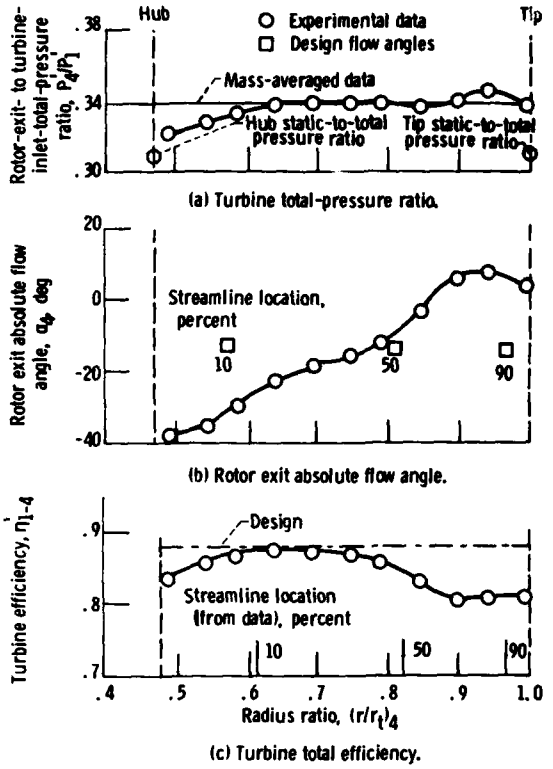

(a) Turbine total-pressure ratio.

(b) Rotor exit absolute flow angle.

(c) Turbine total efficiency.

Figure 17. - Rotor exit radial survey results at corrected design speed and a total-pressure ratio of 3.024.

presented in figure 17(a). The measured static-to-total pressure ratios P_4/P_1' on the hub and tip walls are also shown, along with the mass-averaged total-pressure ratio calculated from the data. Figure 17(a) shows that the rotor exit total pressure was higher than average near the tip and lower than average near the hub. The lower total pressure measured near the hub indicates reduced flow in this region and probably results from the large trailing-edge blockage (78.7 percent at the hub).

The absolute flow angle, shown in figure 17(b), varies more than 45° from hub to tip. This variation is from an angle of -37.3° near the hub to 8.0° near the tip. The design exit flow angles are also shown in figure 17(b) at the 10, 50, and 90 percent streamline locations (based on MERIDL results). The comparison with experiment is not good in the hub and tip regions. Some disagreement should be expected between experiment and design because simplified loss models were used in the design computer codes and because data could be taken at only one circumferential location.

The variation in total efficiency from hub to tip is shown in figure 17(c). Local total efficiency peaked at 0.875 near a radius ratio $(r/r_t)_4$ of 0.65. This peak value is less than the overall design value of 0.88 also shown in figure 17(c). Although both hub and tip regions had lower efficiencies, the larger and more significant drop in efficiency occurred in the tip region. Almost 50 percent of the mass flow passed through this region, as indicated by the location of the 50 percent streamline at a radius ratio of 0.802 in figure 17(c). A large portion of the work output was extracted at the lower efficiency level in the tip region.

Experimental Velocity Diagrams

The experimental velocity diagrams were calculated from the rotor inlet and rotor exit survey data presented in figures 16 and 17, respectively. To simplify these calculations, the stator inlet conditions were assumed to be uniform, and the static-pressure variations between hub and tip at the rotor inlet and the rotor exit were assumed to be linear. The velocity diagrams are shown in figure 18 for the 10, 50, and 90 percent streamlines (denoted hub, mean, and tip, respectively, in the text). The turbine operating point was at design corrected speed and a near-design corrected total-to-static pressure ratio P_1'/P_4 of 3.22.

As shown in figure 18 flow velocities were subsonic throughout. However, the velocity level through the vaneless-space region between stations 2 and 3 was relatively high with a mean critical velocity ratio of 0.893 at the rotor inlet. This velocity level is significantly higher than that of reference 8 (critical velocity ratios of 0.50 to 0.60), which was used to verify the aerodynamic acceptibility of the vaneless-space length during the turbine design effort. Because of the larger surface friction losses associated with higher velocity levels, the maximum acceptable vaneless-space length for this application was probably less than that indicated by reference 8 (also see the section Turbine Design).

Actual rotor inlet incidence is indicated in figure 18 by the relative flow angles β_3, which are 10.0°, 12.3°, and 7.7° for the hub, mean, and tip, respectively. However, the effective incidence at the rotor mean was 49.0° since for design values of tip speed, stator exit flow angle, and rotor blade number the relative flow angle needed to establish optimum rotor inlet flow conditions, based on the "slip" factor correlation presented in reference 5, was -36.7°. The turbine work factor corresponding to these optimum rotor inlet flow conditions was 0.833; the value at survey conditions was 1.060. As shown in figure 14(a) measured peak total efficiency occurred at or near the theoretical optimum work factor.

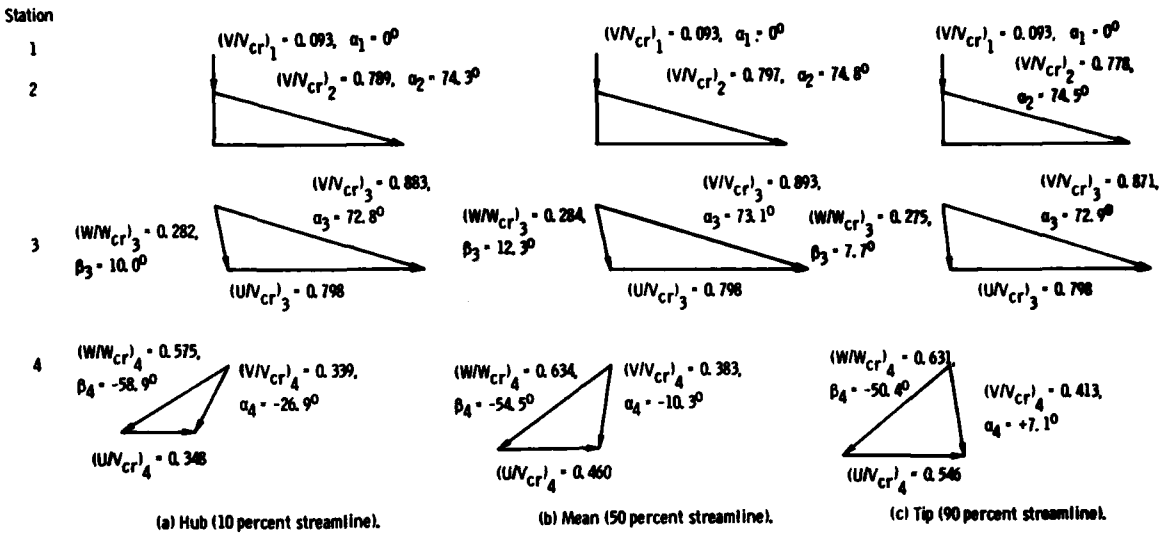

Figure 18. - Experimental velocity diagrams at corrected design values of speed and total-to-total pressure ratio P_1'/P_4'.

The velocity diagrams varied considerably from hub to tip at the rotor exit, with negative swirl at the hub and positive swirl at the tip. This variation is due to the effects of large trailing-edge blockage in the hub region and to possible secondary flows within the rotor. The calculated deviation angles *d* inside the rotor trailing edge were 1.2°, -2.5°, and -8.8° at the hub, mean, and tip, respectively. The large amount of underturning (negative deviation) at the tip may be due to the migration of rotor losses into the tip region. This statement is based on the rotor exit tip clearance being only 1.2 percent of the exit blade height. Reference 11 indicates only a small loss associated with this percentage of tip clearance.

The velocity diagrams also show the effect of the large hub blockage (78.7 percent) on flow distribution from hub to tip. The local axial velocity normalized by the 50-percent-streamline axial velocity $V_x/V_{x,m}$ was 0.80, 1.00, and 1.09 at the hub, mean, and tip streamlines, respectively. This is a further indication that flow was constricted in the hub region by the large trailing-edge blockage.

Internal Losses

The turbine internal losses were investigated with available analytical methods in conjunction with loss calculations based on experimental data. The turbine operating point used for this investigation was at corrected design values of speed and total-to-total pressure ratio P_1'/P_4' and corresponds to the conditions used for the rotor exit radial survey. The turbine total efficiency at this operating point, as based on measured torque and mass flow and on calculated total pressures, was 0.827. This is 5.3 efficiency points less than design.

The stator and vaneless-space loss was measured by the rotor inlet survey as described previously. The mass-averaged total-pressure loss was 6.3 percent, about 3.15 times that assumed in the original design. This measured loss includes the losses due to stator surface friction on the vanes and endwalls, stator secondary flows, stator wake mixing, and vaneless-space surface friction. As stated previously, wake mixing and vaneless-space losses were not specifically included in the design estimate.

Computer programs MERIDL (ref. 6) and TSONIC (ref. 7) were used to obtain the velocity distributions on the stator vanes and endwalls and on the vaneless-space walls. The computer program BLAYER (ref. 12) was then used to obtain the boundary-layer loss parameters. The kinetic energy loss coefficients for the loss mechanisms listed were calculated by the method presented in reference 13. This series of calculations is essentially two dimensional so that secondary flow effects (three-dimensional effects) are not included. Since the stator aspect ratio was 0.265 and there was about 73.6° of flow turning, significant secondary flow losses were expected.

The stator and vaneless-space total-pressure loss of 6.3 percent corresponds to 5.76 points in turbine total efficiency. Figure 19 shows the breakdown of this loss for the various stator loss mechanisms identified as percentages of the total measured loss based on the results of the analytical calculations. Only 54 percent of the total loss was predicted by the analytical methods used. It seems reasonable to

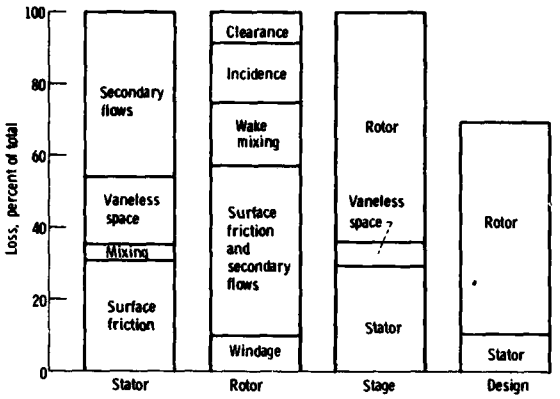

Figure 19. - Breakdown of turbine losses at corrected design values of speed and total-pressure ratio.

assign the remaining 46 percent of the loss to the secondary flow effects that could not be accounted for with this analysis. In terms of efficiency points the losses due to stator vane and endwall surface friction, wake mixing, vaneless-space surface friction, and stator secondary flows were 1.83, 0.46, 1.05, and 2.42 points, respectively. The design value of stator loss, 1.8 efficiency points, agrees well with the calculated stator surface friction loss. The additional losses due to wake mixing, vaneless-space surface friction, and secondary flows were not specifically included in the design loss estimate. However, it is apparent that these losses require careful analysis in high-work-factor radial turbine design. The high calculated vaneless-space surface friction losses are consistent with the high Mach numbers and the long gas path present. The average absolute Mach number at the rotor inlet was about 0.87, and the gas path was 1.5 times the stator chord in length (see the section Experimental Velocity Diagrams).

The total rotor loss was determined by subtracting the measured stator and vaneless-space kinetic energy loss from the stage enthalpy loss. The rotor loss was calculated to be 11.54 efficiency points; the design loss was 10.2 points. Measured rotor losses were 13.1 percent larger than design. The total rotor loss included losses due to surface friction, secondary flows (three-dimensional effects), incidence, wake mixing, tip clearance, and disk windage. The rotor wake mixing losses were calculated with the procedure described previously, which was used to calculate the stator profile and mixing losses. The rotor incidence losses were calculated by assuming that the relative inlet velocity normal to the blading was lost (ref. 14). Rotor tip clearance losses were calculated from the tip clearance correlation presented in reference 11. Finally, the disk windage losses were calculated by using the equation presented in reference 5.

Figure 19 shows the breakdown of these calculated losses identified as percentages of the total measured rotor loss. In terms of turbine efficiency the rotor losses due to clearance, incidence, wake mixing, surface friction and secondary flows, and disk windage were 1.00, 1.95, 2.00, 5.43, and 1.16 points, respectively. The additional wake mixing losses due to the thick trailing edge were not included in the design loss estimate since the trailing-edge ejection of coolant was planned in the hot application. However, these additional mixing losses are the main reason that rotor losses were 13.1 percent larger than design since the other losses were included in the overall efficiency estimate.

The losses due to incidence, surface friction, and secondary flows cannot be separated by using a two-dimensional boundary-layer analysis. The effects of tip clearance on blade loading cannot be predicted quantitatively either. Therefore these losses were calculated separately by empirical methods. Surface friction losses and secondary flow losses are combined in figure 19 for the rotor. The calculated losses for clearances, incidence, wake mixing, and windage are based on theory and correlated data. The remaining loss, based on the measured rotor loss, was then assigned to surface friction and secondary flow effects.

The relative magnitudes of the losses associated with the stator, the vaneless space, and the rotor are illustrated for the turbine stage in figure 19. Although the rotor accounts for 64.2 percent of the measured stage loss, the stator losses of 29.3 percent are a significant fraction of the total loss. In terms of turbine efficiency the losses in the stator, the vaneless space, and the rotor were calculated to be 4.71, 1.05, and 11.54, points respectively. For the turbine design, vaneless-space losses were not accounted for and stator and rotor losses were assumed to be 1.8 and 10.2 efficiency points, respectively.

The investigation of turbine internal losses has been useful in identifying the loss mechanisms resulting in the 5.3-point deficit in measured turbine efficiency as compared with design estimates. In the stator, analytical calculations and test data indicated a 2.42-point penalty from secondary flow effects because of the low (0.265) stator aspect ratio and a 0.46-point penalty because of trailing-edge-wake mixing effects. A 1.05-point penalty from vaneless-space surface friction was calculated analytically and was due to the long gas path and the high Mach number level. In the rotor, analytical calculations indicated a 2.00-point penalty from the wake mixing losses because of the thick rotor trailing edge that was required for coolant ejection in the hot

application. These four losses resulted in a 5.93-point penalty in turbine total efficiency.

The design mixing losses can be estimated by assuming "thin" blading and by recalculating the mixing loss from the velocity diagram data and the analytical results of the preceding analysis. Stator trailing-edge thickness was assumed to be 0.0635 centimeter; rotor trailing-edge thickness was assumed to vary linearly from 0.1524 centimeter at the hub to 0.0635 centimeter at the tip. The total design mixing losses were calculated to be 0.66 efficiency point, evenly divided between stator and rotor. Then the total additional mixing losses due to the thick stator and rotor blading were reduced from 2.46 points to 1.8 points. This reduced the overall calculated penalty in turbine total efficiency to 5.27 points; the measured deficit was 5.3 points.

The design efficiency for the subject radial turbine was based on correlated data from high-efficiency radial turbines with thin blading and "optimum" loading characteristics. However, design compromises to accommodate a high-work-factor, high-inlet-temperature design have resulted in geometry and performance characteristics that differ significantly from those of high-efficiency radial turbines. The turbine geometry characteristics responsible for the low measured efficiency were the reduced rotor tip diameter (high work factor), the low stator aspect ratio (secondary flow effects), the long vaneless space (surface friction losses), and the thick blade trailing edges (wake mixing losses). The turbine test results and subsequent internal loss analyses have shown that geometry compromises can have a significant effect on turbine performance and that the aerodynamic effects of these compromises must be investigated either analytically or experimentally for accurate prediction of design performance.

Summary of Results

The experimental performance of a 15.04-centimeter-tip-diameter, radial-inflow turbine with thick vanes and blades has been determined in air at nominal turbine inlet conditions of 1.379×10^5 N/m^2 and 322.2 K. These conditions yield the design Reynolds number for operation at the corrected design values of mass flow and speed. Data have been obtained at corrected speeds from 0 to 110 percent of design and at turbine-inlet-total- to rotor-exit-static-pressure ratios P_i'/P_4 from 1.2 to 4.7. The overall performance was presented in terms of mass flow, torque, specific work, and efficiency. The results of rotor inlet and rotor exit surveys were presented along with the calculated experimental velocity diagrams. The results of an analytical study to assess internal losses and their effect on turbine performance were also presented. The results obtained are as follows:

1. At corrected design values of speed and turbine-inlet-total- to rotor-exit-static-pressure ratio P_i'/P_4, 3.255, the mass flow was 0.2372 kilogram per second (2.55 percent greater than design) and the torque was 4.702 newton-meters (3.25 percent less than design).

2. The measured total and static efficiencies were 0.827 and 0.788, respectively, at corrected design values of speed and P_i'/P_4. Total efficiency was 5.3 points less than design.

3. The total efficiencies at the design work factor of 1.126 and at the theoretically optimum work factor of 0.833 were 0.824 and 0.842, respectively. Peak efficiency was obtained at this "optimum" work factor.

4. Based on analytical and experimental results the kinetic energy losses for the stator, the vaneless space, and the rotor were 29.3, 6.5, and 64.2 percent of the total stage loss, respectively.

5. The internal loss investigation indicated that the 5.3-point deficit in efficiency was due to the effects of stator secondary flows, vaneless-space surface friction, and wake mixing, with the penalties calculated to be 2.42, 1.05, and 1.80 efficiency points, respectively.

6. This investigation showed that compromises in geometry can significantly affect turbine performance. The aerodynamic effects of these compromises must be investigated either analytically or experimentally for accurate prediction of design performance.

Lewis Research Center
National Aeronautics and Space Administration,
Cleveland, Ohio, April 8, 1980,
505-32.

References

1. Haas, Jeffrey E.; and Kofskey, Milton G.: Cold-Air Performance of a 12.766-Centimeter-Tip-Diameter Axial-Flow Cooled Turbine. I—Design and Performance of a Solid Blade Configuration. NASA TN D-7881, 1975.
2. Haas, Jeffrey E.; and Kofskey, Milton G.: Cold-Air Performance of a 12.766-Centimeter-Tip-Diameter Axial-Flow Cooled Turbine. II—Effect of Air Ejection on Turbine Performance. NASA TP-1018, 1977.
3. Rodgers, C.: Advanced Radial Inflow Turbine Rotor Program: Design and Dynamic Testing. SOLAR-ER-2519, Solar; NASA Contract NAS3-18524.) NASA CR-135080, 1976.

4. Kofskey, Milton G.; and Nusbaum, William J.: Effects of Specific Speed on Experimental Performance of a Radial Inflow Turbine. NASA TN D-6605, 1972.

5. Rohlik, Harold E.: Analytical Determination of Radial Inflow Turbine Design Geometry for Maximum Efficiency. NASA TN D-4384, 1968.

6. Katsanis, Theodore; and McNally, William D.: Revised FORTRAN Program for Calculating Velocities and Streamlines on the Hub-Shroud Midchannel Stream Surface of an Axial-, Radial-, or Mixed-Flow Turbomachine or Annular Duct. I—Users Manual. NASA TN D-8430, 1977.

7. Katsanis, Theodore: FORTRAN Program for Calculating Transonic Velocities on a Blade-to-Blade Stream Surface of a Turbomachine. NASA TN D-5427, 1969.

8. Kofskey, Milton G.; and Haas, Jeffrey E.: Effect of Reducing Rotor Blade Inlet Diameter on the Performance of a 11.66-Centimeter Radial-Inflow Turbine. NASA TM X-2730, 1973.

9. Futral, Samuel M.; and Wasserbauer, Charles A.: Experimental Performance Evaluation of a 4.59-Inch Radial-Inflow Turbine With and Without Splitter Blades. NASA TN D-7015, 1970.

10. Futral, Samuel M.; Kofskey, Milton G.; and Rohlik, Harold E.: Instrumentation Used to Define Performance of Small Size, Low Power Gas Turbines. NASA TM X-52522, 1969.

11. Futral, Samuel M., Jr.; and Holeski, Donald E.: Experimental Results of Varying the Blade-Shroud Clearance in a 6.02-Inch Radial-Inflow Turbine. NASA TN D-5513, 1970.

12. McNally, William D.: FORTRAN Program for Calculating Compressible Laminar and Turbulent Boundary Layers in Arbitrary Pressure Gradients. NASA TN D-5681, 1970.

13. Stewart, Warner L.: Analysis of Two-Dimensional Compressible-Flow Loss Characteristics Downstream of Turbomachine Blade Rows in Terms of Basic Boundary-Layer Characteristics. NACA TN-3515, 1955.

14. Glassman, Arthur J.; ed.: Turbine Design and Application. NASA SP-290 Vol-2, 1973.

1. Report No.	2. Government Accession No.	3. Recipient's Catalog No.
NASA TP-1730 AVRADCOM TR 80-09	AD-A092 120	

4. Title and Subtitle	5. Report Date
EXPERIMENTAL PERFORMANCE AND ANALYSIS OF 15.04-CENTIMETER-TIP-DIAMETER, RADIAL-INFLOW TURBINE WITH WORK FACTOR OF 1.126 AND THICK BLADING	October 1980
	6. Performing Organization Code

7. Author(s)	8. Performing Organization Report No.
Kerry L. McLallin and Jeffrey E. Haas	E-391
	10. Work Unit No. 505-32

9. Performing Organization Name and Address	11. Contract or Grant No.
NASA Lewis Research Center and Propulsion Laboratory AVRADCOM Research and Technology Laboratories Cleveland, OH 44135	

12. Sponsoring Agency Name and Address	13. Type of Report and Period Covered
National Aeronautics and Space Administration Washington, DC 20546 and U.S. Army Aviation Research and Development Command St. Louis, MO 63166	Technical Paper
	14. Sponsoring Agency Code

15. Supplementary Notes

Kerry L. McLallin: Lewis Research Center.

Jeffrey E. Haas: Propulsion Laboratory, AVRADCOM Research and Technology Laboratories.

16. Abstract

The aerodynamic design, the experimental performance, and an internal loss breakdown are presented for a 15.04-cm-tip-diameter, radial-inflow turbine. The design application is to drive a two-stage, 10-to-1 pressure ratio compressor with a mass flow of 0.952 kg/sec and a rotative speed of 70 000 rpm. The turbine inlet temperature was 1478 K, and the turbine was designed with blades thick enough for internal cooling passages. The rotor tip diameter was limited to 86 percent of optimum in order to obtain a reduced-tip-speed design. The turbine was fabricated with solid, uncooled blading and tested in air at nominal inlet pressure and temperature of 1.379×10^5 N/m^2 and 322.2 K, respectively. Experimental results indicated the turbine total efficiency to be 5.3 points less than design. Analysis of these results has indicated the deficit in performance to be due to stator secondary flow losses, vaneless-space surface friction losses, and trailing-edge wake mixing losses.

17. Key Words (Suggested by Author(s))	18. Distribution Statement
Radial-inflow turbine; Turbine cooling; High aerodynamic loading; Experimental performance; Internal losses	Unclassified - unlimited STAR Category 07

19. Security Classif. (of this report)	20. Security Classif. (of this page)	21. No. of Pages	22. Price*
Unclassified	Unclassified	20	A02

* For sale by the National Technical Information Service, Springfield, Virginia 22161

NASA-Langley, 1980